



# The Effect of Laser Irradiation on the Compressive Strength of Granite Under Uniaxial Compression

Bin Xu<sup>1,2</sup> · Xinjie Huang<sup>1,2</sup> · Biao Li<sup>1,3</sup> · Bo Zhang<sup>1,3</sup> · Mengmeng Hu<sup>1,3</sup> · Chuanyi Ma<sup>4</sup> · Chuan Wang<sup>4</sup> · Tongyuan Liu<sup>1,2</sup>

Received: 21 June 2023 / Accepted: 30 October 2023 / Published online: 30 November 2023  
© The Author(s), under exclusive licence to Springer-Verlag GmbH Austria, part of Springer Nature 2023

## Abstract

In order to improve the crushing efficiency of drilling machinery, laser-assisted mechanical rock-breaking technology has gained wide attention in the field of engineering construction. In this method, the weakening effect of the laser on the compressive strength of the rock is a key factor of the technology. To reveal the weakening effect of the laser on the compressive strength of rocks, standard uniaxial compression tests were carried out on irradiated rocks using a uniaxial compression testing machine. The weakening effect of laser power and irradiation time on rock strength and rock failure mode was investigated. The experimental results show that the laser power and irradiation time have similar effects on the mechanical properties of the rocks. With the increase of laser power and irradiation time, the peak stress of the specimens shows a tendency to decrease rapidly and then slowly. At the same time, the rock elastic modulus decreases and peak strain increases, and the behavior eventually transform from brittle damage to plastic damage. Melting pit holes and crack networks are the root cause of the weakness of the compressive strength. On one hand, the vertical melting pit hole provides a conical free surface, which reduces the rock deformation constraint and generates stress concentration at the bottom of the hole, so that it facilitates the splitting-tension damage of the specimen. On the other hand, the axial load induces symmetric tensile cracks in the thermal cracks, and adjacent tensile cracks interpenetrate to create a surface of tensile damage, leading to fragmentation of the specimen in the form of rock blocks, ultimately undermining the rock. This work provides an improved understanding of the effect of lasers on the compressive strength of rocks in engineering applications.

## Highlights

- The effect of laser irradiation on the compressive strength weakening of rock was investigated.
- Failure modes and strength weakening mechanisms of irradiated rocks were revealed.
- The advantage parameters of laser-assisted rock breaking were clarified.

**Keywords** Laser rock breaking · Uniaxial compression · Strength weakening · Failure mode

✉ Biao Li  
libiaosdu@163.com

- <sup>1</sup> Geotechnical and Structural Engineering Research Center, Shandong University, Jinan 250061, Shandong, People's Republic of China
- <sup>2</sup> School of Qilu Transportation, Jinan 250061, Shandong, People's Republic of China
- <sup>3</sup> School of Civil Engineering, Shandong University, Jinan 250061, Shandong, People's Republic of China
- <sup>4</sup> Shandong Hi-Speed Group Co., Ltd, Jinan 250098, Shandong, People's Republic of China

## 1 Introduction

With the vigorous development of the underground space, infrastructure such as transportation construction, water conservation and hydropower have entered a new period of rapid development, and a large number of tunnels, underground facilities, road foundations, slopes and other projects are being or will be built (Maeda and Kushiyama 2005; Zhou and Chen 2019; Zhang et al. 2023). Engineering drilling rigs are one of the most widely used mechanical equipment in the construction of tunnels and underground spaces, and are

used in geological surveys, hydrological surveys and geotechnical construction (anchoring, grouting, drilling, etc.) due to their wide adaptability, high speed, automation and safety (Li et al. 2021b; Khaled et al. 2022). During the process of rock breaking, the drill pipe drives the drill bit to rotate and cut the rock continuously, and the efficiency of rock breaking of the drill bit directly affects the construction efficiency of the drill rig. Therefore, the rock-breaking performance and mechanism of cutting teeth have received a lot of attention from researchers. In general, the conventional cutting teeth rock-breaking mechanism can be described as follows: the cutting teeth squeeze the rock under the action of thrust, then the cutting teeth scrape the rock surface in the form of shear by rotation, and finally form rock chips (Li et al. 2021a). The geological drilling rig can conduct fast drilling work in medium-hard rock environments through the above process.

However, as the mining of earth resources and tunnel excavation encounter stronger rocks, traditional mechanical rock-breaking methods have shown problems such as low rate of penetration (ROP) during drilling operations and high tool wear (Gupta et al. 2013; Capik and Yilmaz 2021), which seriously affects the construction process and is detrimental to the economics of drilling rig construction. For example, in 2017, during the construction of drilling in the Mastakhskaya area (Republic of Sakha (Yakutia), Russia), the drilling rig encountered permafrost, resulting drilling speed to drop by more than half, with an average drilling speed of less than 4 m/h, seriously delaying the construction schedule and significantly increasing the drilling cost (Atlasov et al. 2019). In 2019, during the drilling construction in Shunbei Oilfield, the drilling rig encountered igneous rock with compressive strength up to 195 MPa. The drilling speed of the rig was about 1.05 m/h, and the PDC bit chipped teeth frequently during the drilling process (Liu et al. 2020). In 2018, during the tunnel survey project in YiLi, Xinjiang, the drilling rig encountered strong abrasive quartzite, with severe bit wear and alloy bit life below 0.5 m, resulting in massive damage to the PDC bit, significantly increasing the economic and time costs of drilling construction (Fan 2019).

Exploring new and efficient rock-breaking methods is an important means of solving the above problems (Kirli and Fahrioglu 2019; Xu et al. 2020). New rock-breaking methods such as laser (Wang et al. 2020b; Guo et al. 2022), high-pressure waterjet (Liu et al. 2023; Li et al. 2022a, b), microwaves (Lu et al. 2019; Wang et al. 2020a), particles (Ren et al. 2019; Fang et al. 2021) and electric pulses (Li et al. 2022c; Zhu et al. 2022) have been proposed, which have become the research hotspots and scientific frontiers in the international engineering drilling field. Among the many new rock-breaking methods, the laser is considered to be a highly promising method as a non-contact rock-breaking method with the advantages of high perforation efficiency and easy implementation (Chen et al. 2022a). Studies have

shown that laser-assisted drilling rig construction can effectively improve rock-breaking efficiency, and its drilling speed can be more than 10 times that of traditional drilling rigs (Pooniwala 2006). Laser assisted technology not only can significantly increase the drilling speed, but also can extend the service life of drill bits and drill pipes, which can effectively avoid the occurrence of accidents such as stuck drilling and abnormal wear. Thus, it has high research and application value in the field of engineering drilling.

Li et al. (2019) found that laser irradiation led to a rapid increase in rock temperature, and the rock generated thermal stresses and eventually fractured under the action of a high-gradient temperature field. Chen et al. (2022b) considered that the evolution of internal rock damage during laser-irradiated thermal fracture is an evolving dynamic process, the accumulation and expansion of rock damage is a factor in crack formation. The formation of cracks also led to an increase in the porosity and permeability of the rock. Ndeda et al. (2017) described the thermal fracture process of granite intuitively by numerical simulation method. Due to the different thermal expansion coefficients of the mineral components that make up the rock, it leads to thermal stresses in the rock under the laser action and causes damage, which leads to a decrease in the integrity of the rock. Yin et al. (2015) carried out a study on the effect of heat treatment on the tensile strength of granite, and the results showed that static tensile strength decreased with increasing temperature, and dynamic tensile strength increased and then decreased at a certain temperature. Rui and Zhao (2021) investigated the effect of laser-induced rock damage on the tensile strength of the specimens. Compared with the unirradiated specimens, the laser irradiation produced significant damage to the tested specimens, resulting in a decrease in the tensile strength. Guo et al. (2022) conducted a study using the response surface method to optimize the laser thermal rock-breaking parameters and confirm the weakening effect of laser on rock mechanical properties. The above studies have confirmed the weakening effect of laser on rock mechanical properties, and have verified the effectiveness of laser-assisted rock-breaking technology. During the rock-breaking process of the laser-assisted drilling rig, the cutting teeth penetrate the rock under the thrust of the drilling rod, and then rotate and scrape the rock to form chips. In this process, it is crucial that the rock is crushed and penetrated by the bit (Dai et al. 2021). It has been demonstrated that the penetration efficiency of the cutting teeth is directly related to the uniaxial compressive strength of the rock. As the strength of the rock increases, the penetration ability of the cutting teeth decreases, and the drilling efficiency of the drilling rig decreases (Han et al. 2020). In addition, the uniaxial compression process of the rock is consistent with the process of the drill bit crushing the intrusive rock.

It can provide a direct reference for drilling rock breaking (Cai et al. 2021). Therefore, it is necessary to discuss in detail the effect of laser irradiation on the compressive strength of the rock, and this will play an important role in promoting the development of laser-assisted mechanical rock-breaking technology.

In this study, considering the effect of laser irradiation on the compressive strength of rocks, standard uniaxial compression tests were conducted on Shenyang ultra-hard granite, and this quantified the effect of laser parameters on the compressive strength and deformation of rocks. First, the rocks were pre-treated by irradiation on a laser rock-breaking test platform, then irradiated specimens were compressed using a uniaxial compression test. Second, the internal crack expansion behavior and strength weakening mechanism of rocks under the action of melting pit holes and crack networks were clarified. Finally, the rock failure modes in the melting pit dominant mode and thermal cracks dominant mode were analyzed, and this would provide engineering guidance and suggestions for the selection of laser parameters to assist the bit in rock breaking.

## 2 Experimental Procedure

### 2.1 Specimen Preparation

The material used is granite collected from Shenyang city in Liaoning Province, which is used to investigate the mechanical and thermal damage behavior of irradiated rock. In this experiment, all specimens are taken from the same rock, and the specimen size is  $\Phi 50 \times 100$  mm. Before the experiment starts, the end face of the specimen is polished with an angle grinder and sandpaper to ensure that they are flat within 0.02 mm, as shown in Fig. 1.

### 2.2 Laser Irradiation Granite Specimen Test

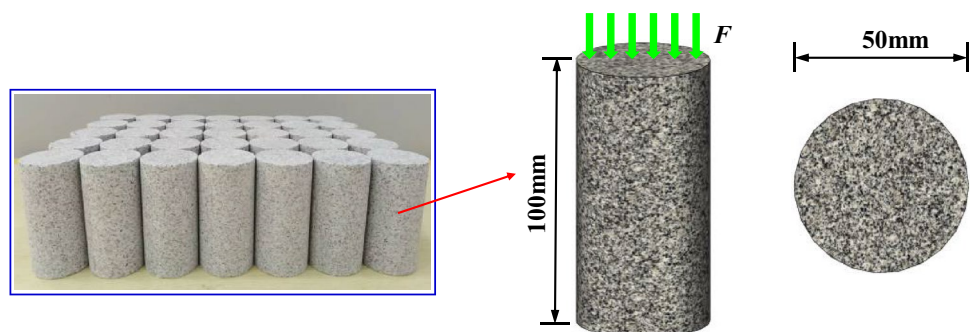
The laser rock-breaking test platform used in this test is mainly composed of a continuous semiconductor laser and a

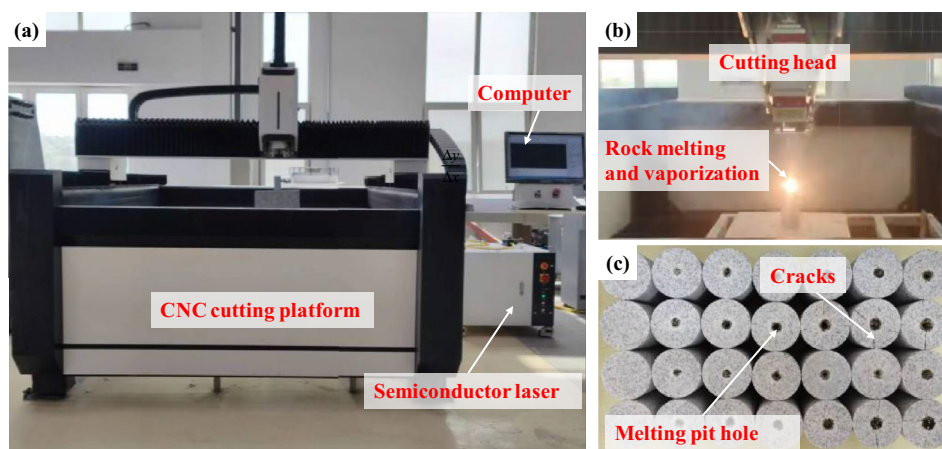
three-axis CNC cutting platform, and the overall structure is shown in Fig. 2a. The laser has a maximum power of 5 kW and a wavelength of 915 nm, and the CNC cutting platform adopts a gantry type of mechanical structure, which allows for three-dimensional spatial adjustment of the cutting head position, the maximum travel of X axis is 1550 mm, Y axis is 1550 mm, Z axis is 150 mm, and the repeat positioning accuracy can reach  $\pm 0.02$  mm. The test platform is systematically controlled through a visual human-machine interface, which allows direct setting and adjustment of the laser power, irradiation time, duty cycle, pulse frequency, laser-specimen relative position, laser cutting track, etc. facilitating the smooth conduct of the test. As shown in Fig. 2b, the specimen is placed on the laser rock-breaking test platform, and a continuous laser with a frequency of 5000 Hz is selected to drill holes in the center of the rock end face. The laser power was 0 W, 800 W, 1600 W, 2400 W, 3200 W, 4000 W, 4800 W, and the irradiation time was set to 5 s and 10 s. Irradiated specimens are shown in Fig. 2c. In order to eliminate the influence of the specimen differences on the test conclusions, each group of tests was carried out three times to take the average value. The specific laser parameters and test results are shown in Table 1.

### 2.3 Uniaxial Compression Granite Specimen Test

Uniaxial compression tests are carried out on laser-irradiated rock specimens as shown in Fig. 3. The main cylinder at the lower end of the uniaxial compression testing machine can apply a maximum static load of 1050 kN. Before the test, applies lubricant to the end surface of the specimen to eliminate the end surface effect. During the test, first, the stress control method is adopted, and the stress is applied to the set value at a rate of 0.5 MPa/s to make it pre-contact. Then the displacement control method is used to load the specimen to failure at a rate of 0.3 mm/min. Data, such as stress and strain, are collected in real-time during the experiment to analyze the impact of laser irradiation on the compressive strength of granite.

**Fig. 1** Geometry of granite specimens from Shenyang, Liaoning Province, China



**Fig. 2** Laser rock-breaking test platform**Table 1** Laser rock-breaking parameters and test results

Rock type	Specimen number	Laser power (W)	Irradiation time (s)	Focal length (mm)	Density (g/cm <sup>3</sup> )	Young's modulus (GPa)	Uniaxial compressive strength (MPa)
Granite	GS#1	0	5	200	2.612	88.3	139.7
	GS#2	800	5			90.7	137.3
	GS#3	1600	5			83.1	115.5
	GS#4	2400	5			76.4	113.1
	GS#5	3200	5			69.3	104.2
	GS#6	4000	5			66.5	97.0
	GS#7	4800	5			57.8	80.2
	GS#8	0	10			88.3	139.7
	GS#9	800	10			98.0	131.1
	GS#10	1600	10			62.1	86.3
	GS#11	2400	10			50.1	80.2
	GS#12	3200	10			54.5	71.6
	GS#13	4000	10			39.3	59.6
	GS#14	4800	10			37.2	49.0

### 3 Results

#### 3.1 Influence of Laser Radiation on the Stress–Strain Curves of Granite

Figure 4a shows the axial stress–strain curves of granite specimens at different laser power conditions, and the irradiation time of the specimens is 10 s. As can be seen from the figure, the stress–strain curves variation characteristics of granite under different laser power conditions are quite different. When the laser power is below 800 W, the stress–strain curve of granite exhibits the following three stages: (1) in the compaction stage, the curves exhibit non-linear fluctuations, which are caused by the gradual compression and closure of the cracks inside the specimen,

and the curves usually show a concave upward trend with increasing strain. (2) In the elastic deformation and yielding stage, after the microcrack closure, the stress–strain curve of granite enters the elastic deformation stage, and the curve grows in an approximately linear trend. With increasing axial deformation, the curve begins to deviate from the linear behavior, which signals the yielding of the specimen. (3) In the post-peak deformation phase, the specimen reaches the peak strength and then enters the post-peak deformation phase. With the increase of axial strain, the axial stress decreases quickly and the rock failure is rapid. The above damage processes are basically the same as those for unirradiated specimens (Zhao 2016; Yang et al. 2017). When the laser power is higher than 800 W, the stress–strain curves characteristics of granite are as follows: (1) in the

**Fig. 3** Uniaxial compression test

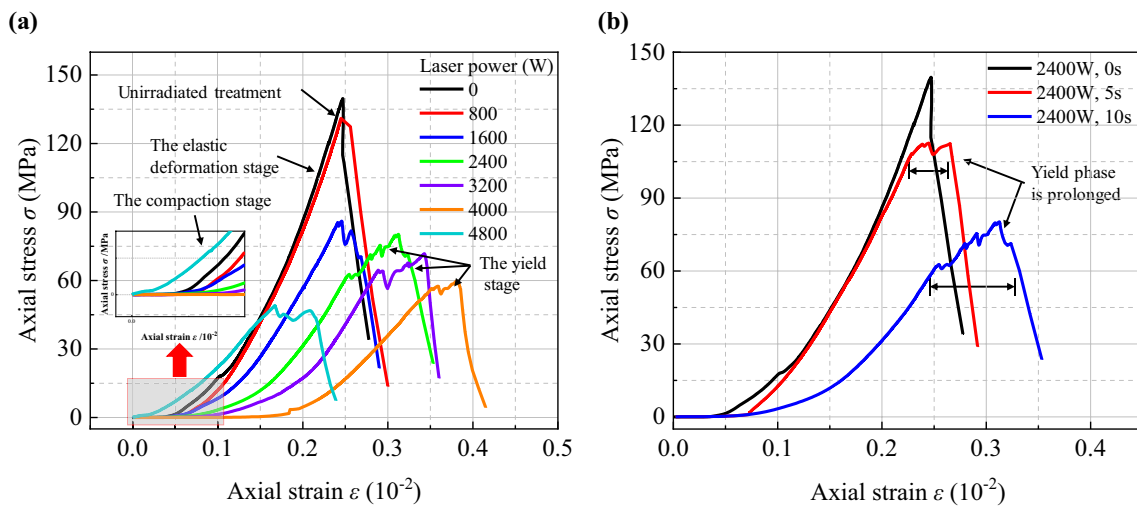
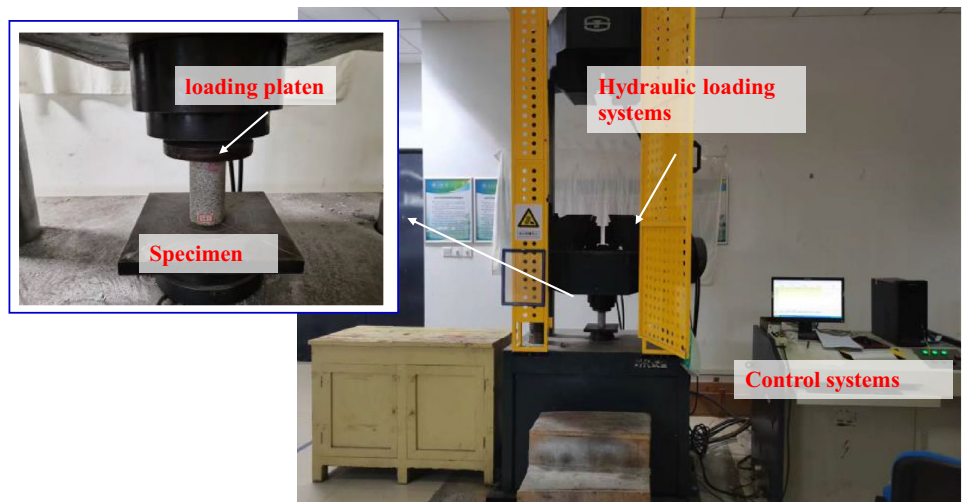


**Fig. 4** Effect of laser radiation on the stress–strain curves of granite. **a** Laser power, **b** irradiation time

compaction stage, with the increase of laser power, the compaction phase of the irradiated specimens is extended and the initial nonlinear deformation becomes more and more significant. This is due to the increasing volume of the melting pit hole produced by the irradiated specimens and the increasing number of thermal cracks, so that the more open microcrack closure leads to larger deformations for small axial loads. (2) In the elastic deformation and yielding stage, the stress–strain curve enters the elastic deformation stage after the microcrack closure, The curve rises in an approximately linear trend. It is obvious that the slope of the curve decreases as the laser power increases. With the increase of axial deformation, the curve enters the yielding stage. It can be seen from the figure that the rock specimen shows a longer nonlinear fluctuation in the yielding phase, and as the laser power increases, the yielding phase before the rock reaches the peak strength is subsequently prolonged. On the

contrary, no significant deformation yielding is observed at laser power of 0 W and 800 W, and the stress–strain curve in the elastic deformation phase extends in an almost linear trend up to the peak point of the specimen. (3) In the post-peak deformation phase, the specimen reaches the peak strength and enters the post-peak deformation stage, with the increase of axial strain, the slope of the curve is slowing, and the rock can be damaged only after certain deformation, and this is different from the rapid splitting failure of the low-power laser-irradiated specimen. Overall, the deformation of the specimen becomes increasingly important as the laser power increases, and this indicates that the behavior changes from brittle damage to plastic damage. However, the change in the stress–strain curve under the laser power of 4800 W is slightly different; this is due to the large number of thermal cracks on the surface and inside the granite specimen caused by the high laser power irradiation, and the specimen

spalling in blocks under axial load, so the compaction stage is significantly reduced.

Figure 4b shows the axial stress–strain curves of granite specimens at different irradiation time conditions, and the irradiation power of the specimens is 2400 W. The axial stress–strain curves of granite at different irradiation times are as follows: (1) in the compaction stage, the compaction phase extends as the irradiation time increases. This is because the longer irradiation time causes the rock to absorb more energy, and the number of thermal cracks in the rock increases, so that the more open microcrack closure leads to larger deformations for small axial loads. (2) In the elastic deformation and yielding stage, after the microcrack closure, the stress–strain curve enters the elastic deformation phase, and the curve rises in an approximately linear trend. It is obvious that the slope of the curve decreases with the increase of irradiation time. With the increase of axial deformation, the curve enters the yielding phase. It can be seen that the rock specimens under irradiation 5 s and 10 s conditions show longer nonlinear fluctuations in the yielding phase, and the longer the irradiation time, the longer the duration of the yielding phase. On the contrary, no significant deformation yield phase is observed at irradiation time of 0 s, and the stress–strain curve in the elastic deformation phase extends in an almost linear trend up to the peak point of the specimen. (3) In the post-peak deformation phase, as the irradiation time increases, the curve of the post-peak deformation phase decreases at a slow rate, and the rock is damaged only after a certain deformation, this is different from the rapid splitting failure of unirradiated specimens. Overall, the deformation of the specimen becomes more and more significant as the irradiation time increases, and this indicates that the behaviour changes from brittle damage to plastic damage.

### 3.2 Influence of Laser Radiation on Peak Stress and Peak Strain of Granite

Figure 5a shows the effect of laser power on the peak stress and peak strain of the specimen, and the irradiation time of the specimens is 10 s. It can be observed that with the increase of laser power, the peak stress of the irradiated specimens shows a significant downward trend. The peak stress of the irradiated specimens decreases faster when the laser power is between 0 and 1600 W. When the laser power is between 1600 and 4800 W, the peak stress of the irradiated specimens decreases gradually with an approximately linear trend. Specifically, when the laser power is increased from 0 to 4800 W, the peak stress of the rock is reduced from 139.7 MPa to 49.0 MPa, with a reduction rate of about 64.9%. It is worth noting that the peak stress drops the fastest at 1600 W, which indicates that 1600 W can produce a desirable weakening effect on rocks. The deformation of the specimens is also closely related to the laser power, and generally there is a law between laser power and rock peak strain as follows: When the laser power is between 0 and 1600 W, the peak strain of the irradiated specimen remains essentially unchanged, however, as the laser power continues to increase (1600 W–4000 W), the peak strain shows an approximately linear increase, and the damage mode of rocks gradually changes from brittle damage to plastic damage. The above phenomenon indicates that there is a damage threshold for the deformation of the specimen. When the energy absorbed by the specimen does not reach the threshold, the specimen remains brittle and the peak strain hardly changes, when the energy absorbed by the specimen exceeds the damage threshold, the behavior of the specimen change and the plasticity becomes more and more obvious as the laser power increases. It should be pointed out that when the laser power reaches 4800 W, the

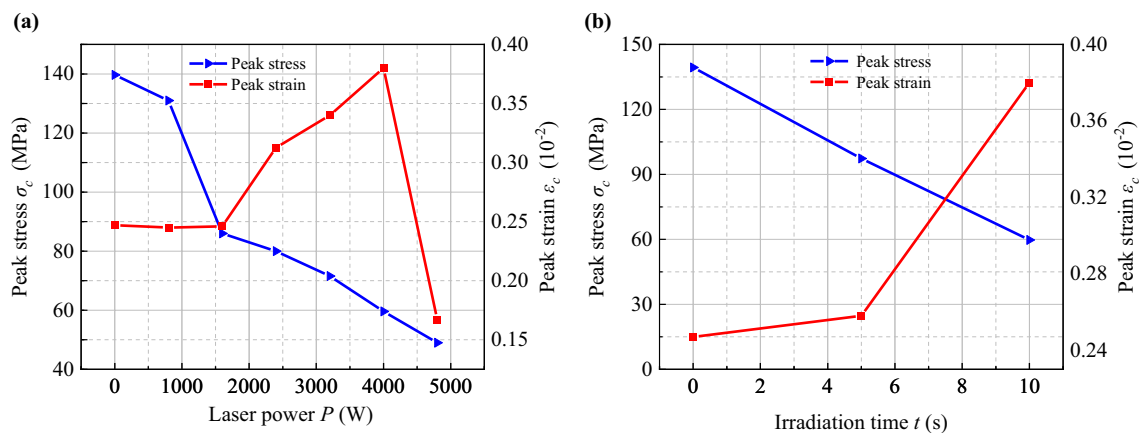


**Fig. 5** Effect of laser radiation on the peak stress and peak strain of granite. **a** Laser power, **b** irradiation time

irradiated specimen produces thermal damage fracture surfaces, and the specimen has formed block spalling before the splitting-tensile damage occurs, this leads to a rapid decrease of the peak strain.

Figure 5b shows the effect of irradiation time on the peak stress and peak strain of granite specimens, and the irradiation power of the specimens is 2400 W. With the increase of irradiation time, the peak stress of the specimens shows an approximate linear decreasing trend. From 0 to 10 s, the peak stress decreases from 139.7 MPa to 80.2 MPa, and the reduction rate is 42.6%. The increase in irradiation time results in a slow, followed by a rapid increase in peak strain, similar to the influence of laser power on the peak strain, and the increasing trend also indicates the existence of a damage threshold. When the irradiation time is short (5 s), the laser output energy is limited, and the threshold value has not been reached, the rock properties do not change and the peak strain growth is small. As the irradiation time increases (10 s), the energy absorbed by the specimen exceeds the threshold value, and the internal damage to the specimen becomes significant, resulting in a transformation of the behavior into plasticity and a noteworthy increase in deformation.

### 3.3 Influence of Laser Radiation on the Elastic Modulus of Granite

The elastic modulus is one of the important parameters in rock mechanics that reflects the physical and mechanical properties of rock materials. The higher the elastic modulus, the better the rock's ability to resist deformation and the greater the difficulty in being destroyed (Martin and Chandler 1994; Yang et al. 2016). The average slope of the elastic deformation straight segment of the stress–strain curve is used as the elastic modulus value (Zhou et al. 2020).

Figure 6a shows the effect of laser power on  $E_{\text{Laser}}$  for irradiation time of 10 s. It can be seen that with the increase of laser power, the elastic modulus of granite shows a trend of rapid decrease and then a slow decrease. When the laser power is less than 2400 W, the elastic modulus of the specimen decreases rapidly with the increase of laser power. Taking the laser power of 2400 W as an example,  $E_{\text{Laser}}$  decreases to 50.1 GPa at this time, and the decrease rate is 43.3%. When the laser power is greater than 2400 W, the elastic modulus of the specimen decreases slower with the laser power increase, and when the laser power increases to 4800 W,  $E_{\text{Laser}}$  decreases from 88.3 GPa to 37.2 GPa, the decrease rate is 57.9%. Figure 6b shows the effect of irradiation time on  $E_{\text{Laser}}$  for laser power of 2400 W. It can be seen that with the increase of laser power, the elastic modulus of granite shows a trend of slow decrease and then rapid decrease. For instance, when the irradiation time is 5 s,  $E_{\text{Laser}}$  slowly decreases to 76.4 GPa, and the decrease rate is only 13.5%. However, when the irradiation time increases to 10 s,  $E_{\text{Laser}}$  decreases rapidly to 50.1 GPa, and the decrease rate is 43.3%. In a word, the elastic modulus tends to decrease rapidly and then slowly with the increase of laser power, while the irradiation time has a different effect on the elastic modulus, and the elastic modulus tends to decrease slowly and then rapidly with the increase of irradiation time.

## 4 Analysis of the Failure Mode and Mechanism of Irradiated Rocks

### 4.1 Drilling Morphology of the Irradiated Rock

As shown in Fig. 7, the specimen forms melting pit hole and crack network under the laser irradiation. When the

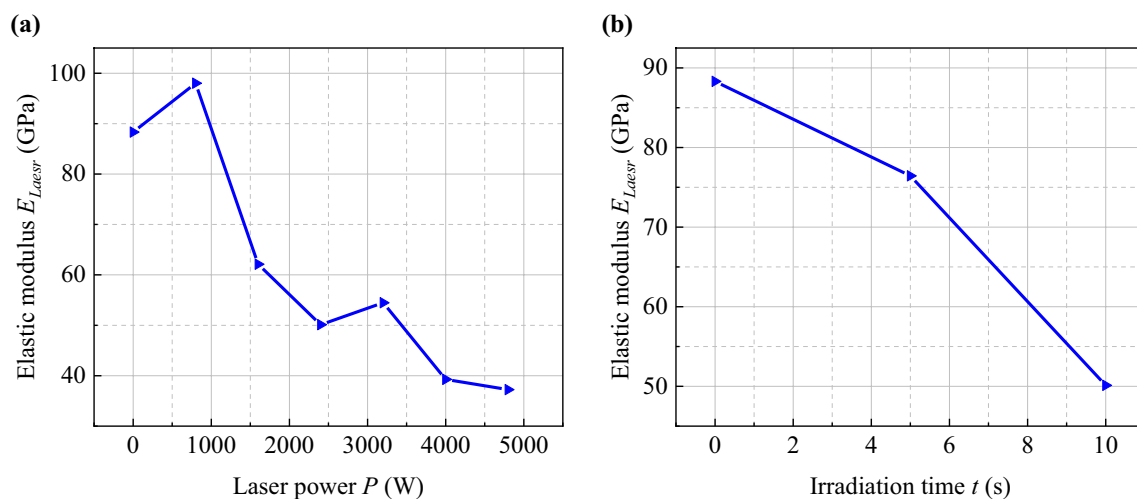
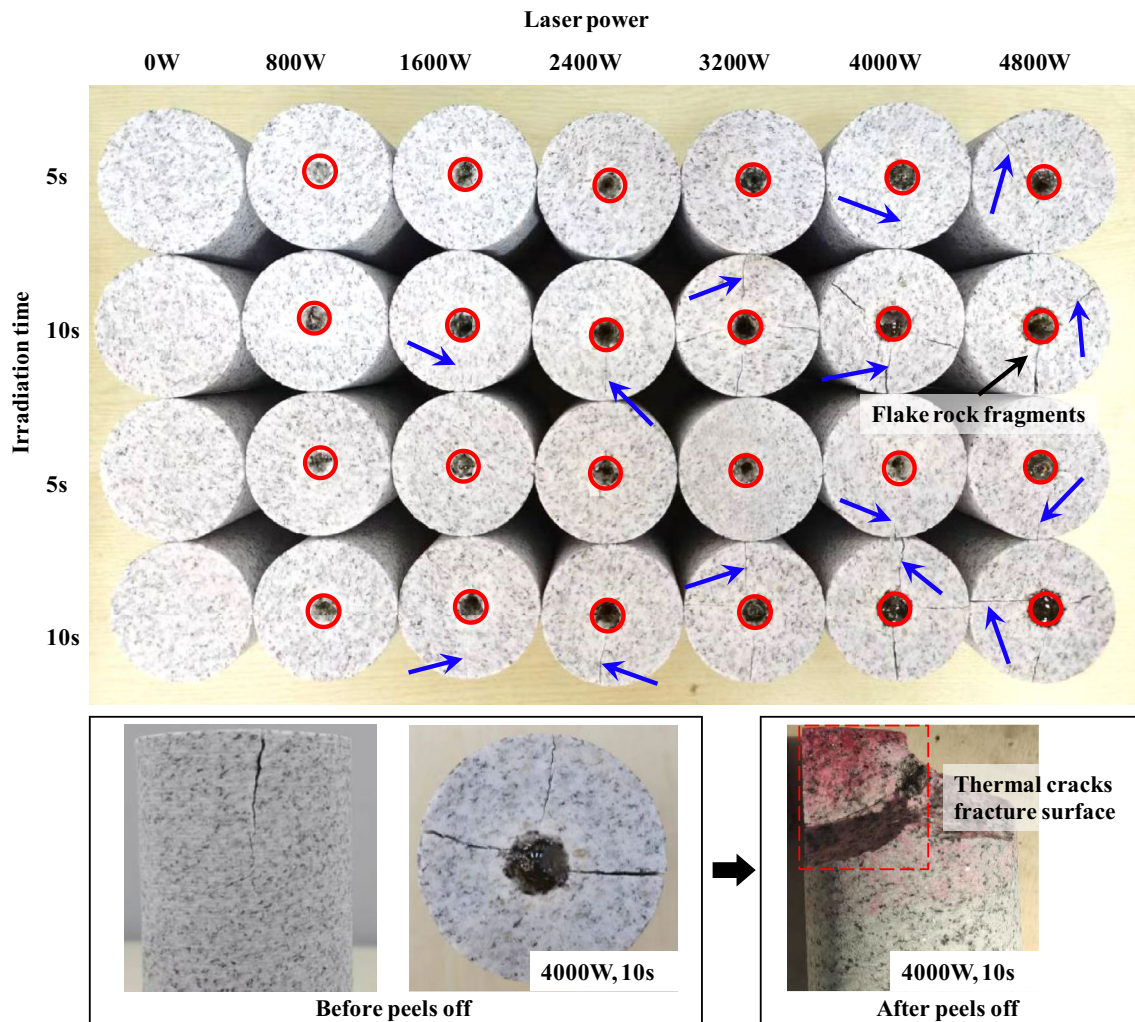


Fig. 6 Effect of laser radiation on the modulus of elasticity of granite. a Laser power, b irradiation time

irradiation time was 5 s, and the laser power was from 0 to 3200 W, the irradiated specimens formed melting pit holes with a few microcracks around the holes, which were caused by the thermal stress resulting from the high temperature. The laser power was between 4000 and 4800 W, the volume of the melting pit hole was increasing under the effect of melting and vaporization, and the shape was approximately inverted cone. Many microcracks were closely distributed around the holes, and the microcracks were continuously expanded and penetrated under the thermal stress, forming 2–3 macro-cracks along the radial expansion, however, the short irradiation time resulted in a small crack width. When the irradiation time was 10 s, and the laser power was from 0 to 1600 W, only melting pit holes were formed, but the hole depth was significantly higher than the depth under the 5 s condition. The laser power ranged from 2400 to 4800 W, and the volume of the melting pit holes continued to expand, accompanied by many tensile cracks around the holes. The

microcracks developed and penetrated with the increase of laser power, eventually forming 3–4 macro-cracks extending along the radial direction, and the crack width increases due to the relatively long irradiation time. It was of concern that when the laser power was 4800 W, due to the interconnection and penetration of microcracks in the heat-affected zone, flake rock spalling was formed on the end face of the specimen, this results in a prolonged compaction phase of the rock stress–strain curve and a rapid decrease in the modulus of elasticity. This also explains the change in the rock specimen stress–strain curve under 4800 W laser power conditions.

In order to quantitatively discuss the effect of laser power on the morphology of melting pit hole, the diameters of the melting pits and heat-affected metamorphic zone circles on the rock irradiation end face are, respectively, defined as the diameters of the melting pits and heat-affected zone of the specimen. Figure 8 shows the behavior of melting pit depth,



**Fig. 7** Irradiated granite specimens (The red circles represent melting pit holes, and the blue arrows represent crack networks)



melting pit diameter and heat-affected zone diameter with laser power. The depth of the melting pit hole approximately trends linearly increasing with the laser power in Fig. 8a. When the irradiation time was 5 s, the depth of the melting pit increased to 19.5 mm from 0 to 4800 W. When the irradiation time was 10 s, the depth of the melting pit increased to 29.3 mm. It was shown that the hole depth under irradiation 10 s increased faster, and the maximum depth was 1.5 times of the hole depth under irradiation 5 s, so an appropriate increase in irradiation time can effectively improve the drilling efficiency. However, the rate of drilling was not always fast. During the test, it was found that as the laser power and irradiation time increased, the molten medium inside the melting pit hole was difficult to remove in time by the auxiliary gas, resulting in more and more glass glaze accumulating in the hole, and this would absorb and reflect more energy, leading to a decrease in the drilling rate.

As shown in Fig. 8b, c, with the increase of laser power, both the melting pit hole diameter and the heat-affected zone diameter show the same logarithmic increasing trend. When the irradiation time was 5 s, the diameter of the melting pit increased from 7.5 mm to 10.8 mm and the diameter of the heat-affected zone increased from 15.2 mm to 22.4 mm from 0 to 4800 W. When the irradiation time was 10 s, the diameter of the melting pit increased from 8.6 mm to 13.2 mm and the diameter of the heat-affected zone increased from 17.7 mm to 27.2 mm. The growth rate of the melting pit diameter and heat-affected zone diameter was slow despite the obvious change in laser power, and the reason was that the small thermal conductivity of the rock samples, so the gradient of the temperature field along the radial direction of the rock is large and the heat is difficult to propagate. As the laser power increases the rock inside the heat-affected zone gradually changed from white to yellow, and this is due to heat accumulation in the heat-affected zone leading

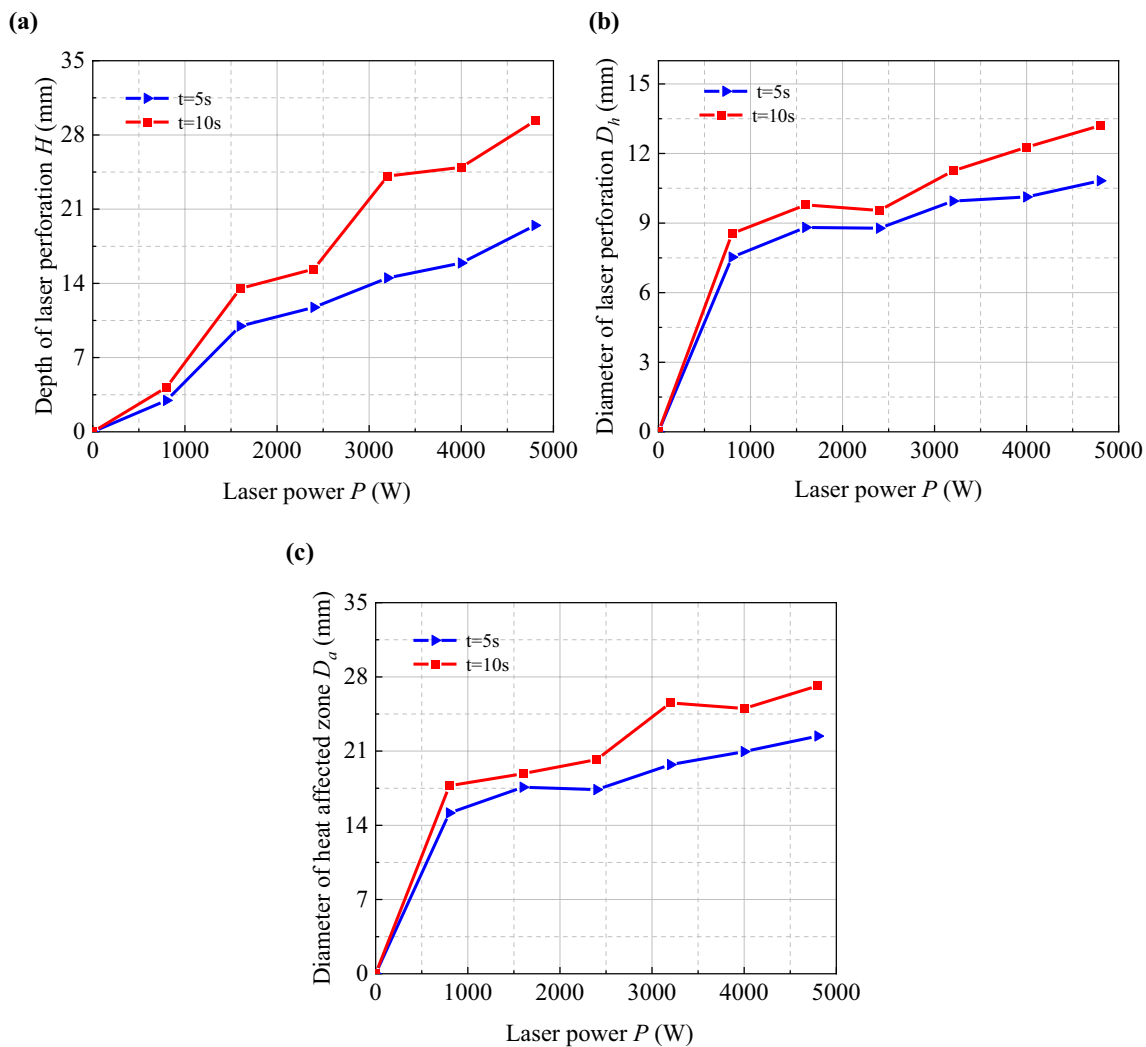


**Fig. 8** Effect of laser power on the melting pit shape. **a** Depth of perforation, **b** diameter of perforation, **c** diameter of affected zone

to mineral dehydration and internal lattice reorganization. It was also observed that the microcracks around the melting pit holes were intensifying to form macro-cracks and even flake rock spalling, which were caused by thermal stress damage. As an approximation, the hole depth could be used to evaluate the volume.

## 4.2 Crack Evolution

In order to further discuss the evolutionary characteristics of cracks on the specimen surface, the irradiated surface is selected as the test surface, and the fractal theory is used to characterize the macro-cracks distribution of the specimen. Before calculating the fractal dimension, the cracks have been extracted from the specimen end face. Digital image processing technology is used to convert end-face photographs of irradiated specimens into binary images, then carries out multiple filtering and denoising processes on the binary images with the help of MATLAB software, and the crack extension paths on the specimen end surfaces are finally obtained with maximum preservation of the crack morphology in Fig. 9. As shown in Fig. 9a, When the laser power is 800 W, the melting pit hole is formed in the center of the specimen, a small number of microcracks appeared around the hole, and no macro-cracks are observed extending to the specimen boundary. When the laser power is increased, the microcracks around the melting pit holes further increases in Fig. 9b and c, and 4–5 macro-cracks are formed through the specimen boundary. With the further increase of laser power, the width and complexity of the macro-cracks penetrating to the specimen boundary increases, multiple secondary cracks are born at the edge of

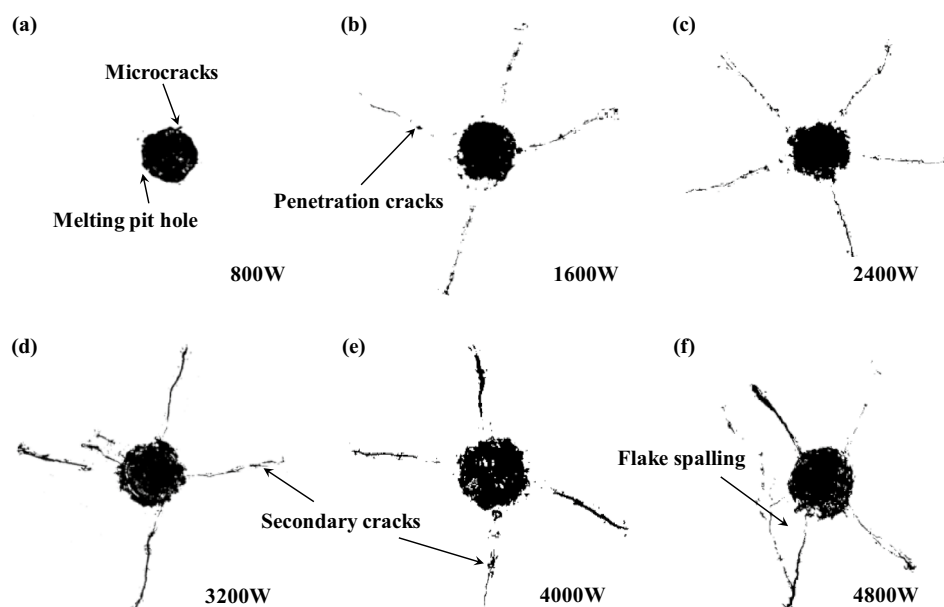
the main cracks in Fig. 9d, e. When the laser power reaches 4800 W, flake spalling is formed between the cracks on the end faces as shown in Fig. 9f.

The box-counting algorithm was widely used in the calculation of the fractal dimension of complex irregular shapes, and the algorithm could well describe the irregularity of rock fracture surfaces (Li et al. 2009). For a given fracture surface  $F$ , in order to find the box-counting dimension of  $F$ , the set could be overlapped by a box with side length  $\epsilon$ , and the total number  $N(\epsilon)$  of required boxes were counted. The fractal dimension  $D$  of the fracture surface  $F$  can be calculated as Eq. (1) (Ai et al. 2014; Allaart and Jones 2023). To easily obtain the fractal dimension, the total number of boxes  $N(\epsilon)$  and the box side length  $\epsilon$  were given as a straight line with slope  $-D$  using a simple logarithmic transformation of the power law. It should be noted that the box-counting method focuses on calculating the total number of boxes that completely cover the set of cracks:

$$D = -\lim_{\epsilon \rightarrow 0} \frac{\log N(\epsilon)}{\log \epsilon} \quad (1)$$

Figure 10 shows the fractal dimension of the cracks on the end face of the specimen, which are 1.2058, 1.3361, 1.3722, 1.4083, 1.4541, and 1.4572 for the end face of the specimen with 800 W, 1600 W, 2400 W, 3200 W, 4000 W, and 4800 W at 10 s of irradiation. The fractal dimension of the irradiated end face is relatively large (generally between 1.2 and 1.5), indicating that the crack distribution on the end face of the irradiated specimen is relatively dispersed, and the crack morphology is highly complex. Further, the relationship between fractal dimension and laser power

**Fig. 9** Crack extension characteristics of the specimen



is plotted in Fig. 11. It is noticed that the fractal dimension increases with the increase of the laser power, which means that the crack complexity also increases. Interestingly,

the fractal dimension seems to rise logarithmically, growing faster when the laser power is below 2400 W and the growth rate slows down when the laser power exceeds 2400

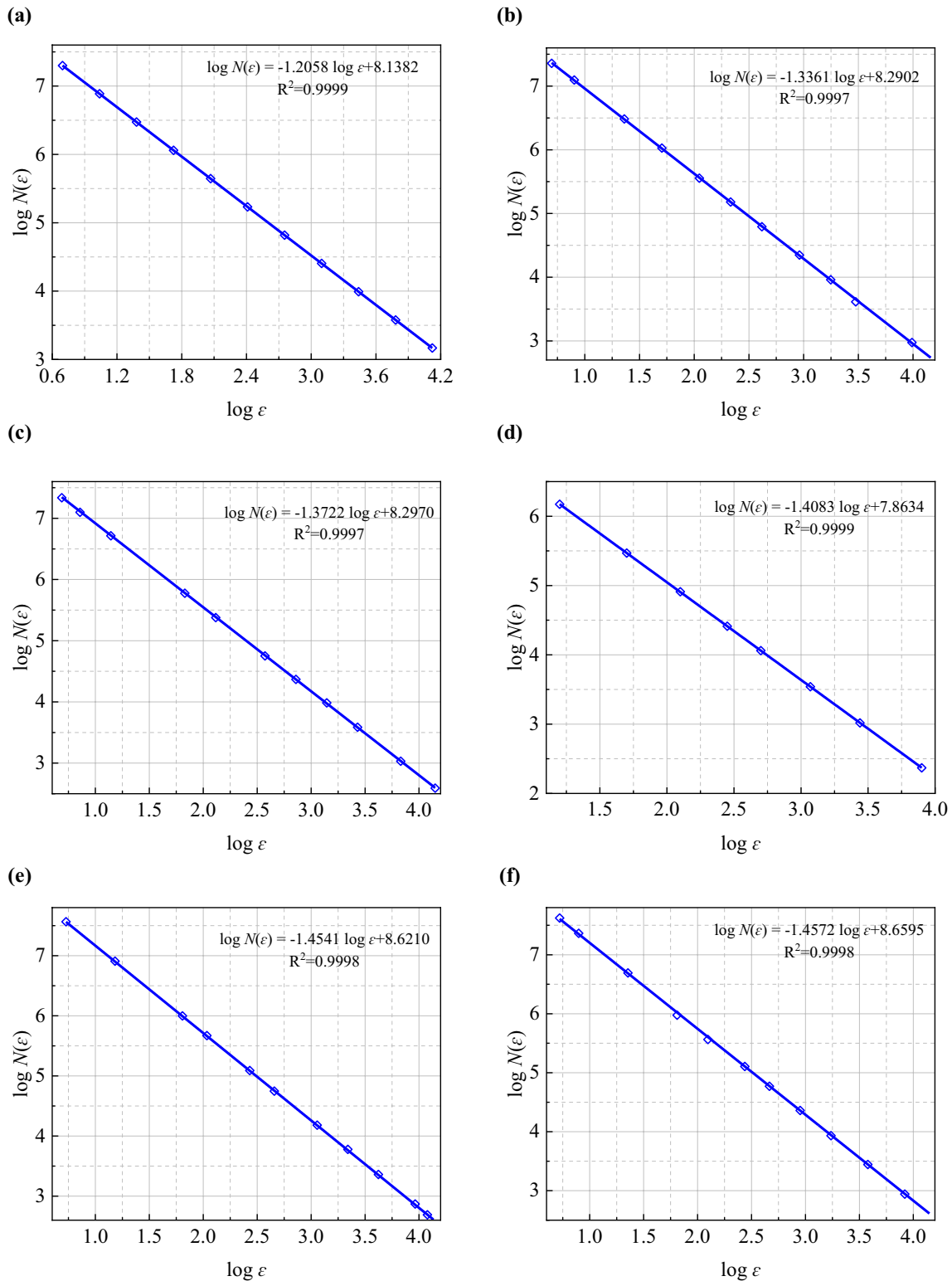


Fig. 10 Fractal dimension of cracks at the specimen end face

W. Therefore, the 2400 W laser power is the turning point of the fast to slow growth rate of the specimen end-face fractal dimension.

### 4.3 Compression Failure Mode and Mechanism of the Irradiated Rock

The laser irradiation has a significant effect on the compressive strength of granite specimens, which is mainly attributed to the generation of melting pit hole and crack network after irradiation, both of which accelerate the development of cracks inside the specimens. When the laser power does not exceed 2400 W, the fractal dimension is small, which indicates that the number and complexity of cracks on the end face of the specimen are small. Figure 12 also shows the cracking on the side of the specimen: when the laser power is 0–1600 W, there is no macro-crack on the side of the specimen, and when the laser power is 2400 W, there is only a small macroscopic crack on the side of the specimen. Therefore, it can be assumed that the damage caused by laser irradiation is mainly the melting pit holes. The hole forms by melting and vaporization can be considered as a conical free surface, where the free surface reduces the internal rock confining stresses and provides free space, resulting in stress concentration at the tip of the hole for the loads distributed on the specimen end faces (Lu et al. 2013; Zhou et al. 2021). Since the tensile strength of the rock is much lower than its compressive strength, the rock area around the hole is the first to form a tensile damage zone. As shown in Figs. 13 and 15a, with the increasing compressive load, the micro-cracks in the tensile damage zone expand and develop and penetrate each other, and the irradiated specimens eventually undergo vertical splitting-tensile damage induced by the conical melting pit holes, which leads to the decrease of the compressive strength of the rock.

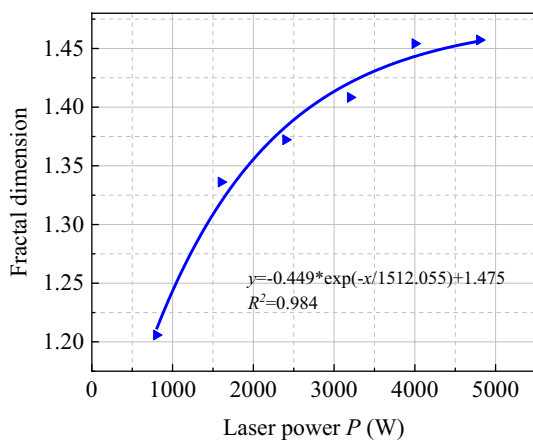


Fig. 11 Relationship between laser power and fractal dimension

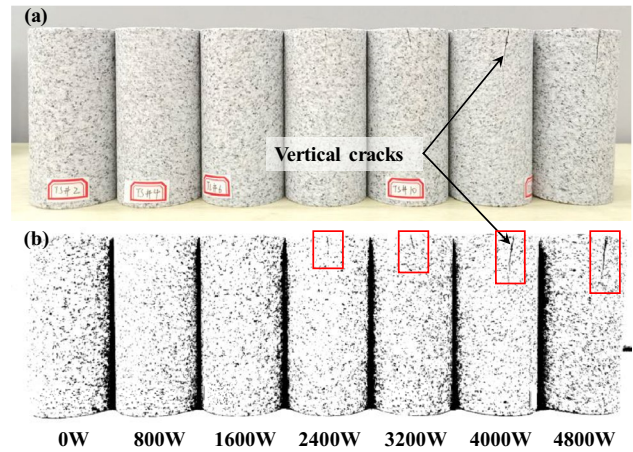


Fig. 12 Crack extension on the side of the specimen. a Original image, b binary image

When the laser power is high than 2400 W, the fractal dimension is larger, indicating that the number and complexity of cracks on the end face of the specimen are large, as well as long macro-cracks occur on the side of the specimen. Therefore, the integrity of the specimen is poor and it can be assumed that the damage caused by laser irradiation is mainly thermal cracks. As shown in Fig. 14, the high-energy laser thermal irradiation causes thermal cracks on the end and sides of the specimens, and multiple thermal damage fracture surfaces are formed inside the specimens. The internal fracture surfaces of the specimens can be viewed as the original defects or damage, so the problem of thermal cracks is transformed into a problem of crack evolution in the specimens with flaws. It is found that the thermal cracks inside the specimen are affected by end stress, which results in the formation of tensile stress concentrations in the middle region of the thermal crack and compressive stress concentrations at the end of the thermal crack due to the specimen end load. With the continuous load applies, the thermal cracks

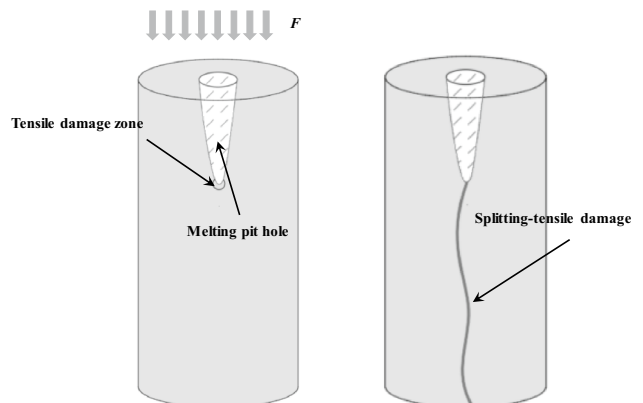
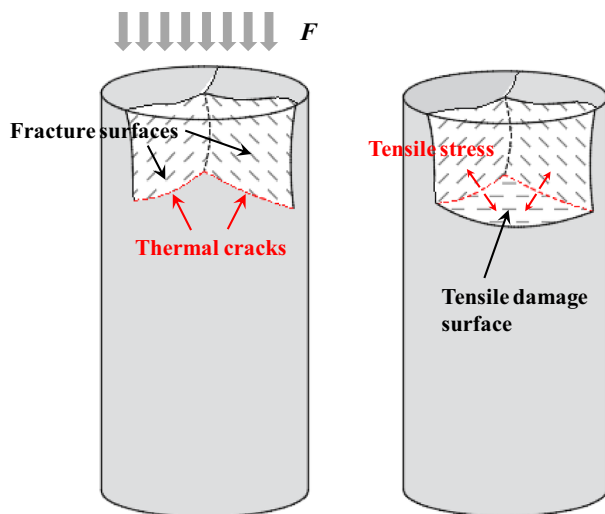


Fig. 13 Internal cracks expansion dominated by melting pit



**Fig. 14** Internal cracks expansion dominated by thermal cracks

are the first to produce symmetric tensile cracks and form damage. Further, the tensile cracks within the two adjacent fracture surfaces penetrate each other to form a tensile damage surface. In addition, the characteristics of the rock block spalling in Fig. 15b indicates that the fracture morphology is relatively rough without shear scratches, and this is consistent with the characteristics of the rock tensile failure discovered by Li et al. (2022b).

In summary, when the laser power did not exceed 2400 W, the effect of melting pit holes on the specimen was greater than the effect of thermal cracks, defining the failure mode at this point as the melting pit dominant mode. In this mode, the specimen was more likely to suffer axial splitting-tension damage. When the laser power exceeded 2400 W, the effect of thermal cracks on the specimen gradually became greater than the effect of melting pit holes, defining this

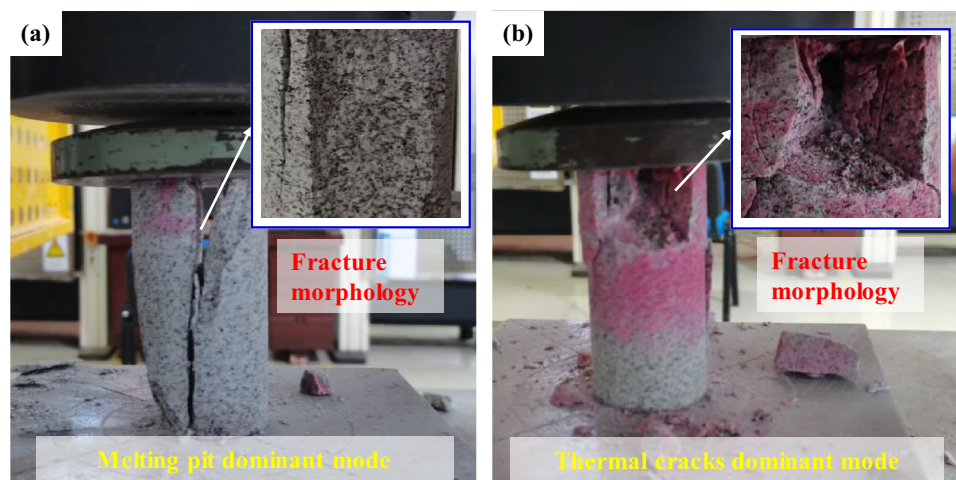
failure mode as the thermal cracks dominant mode. In this mode, the specimen underwent block spalling damage, and this led to a further reduction in the compressive strength of the specimen.

## 5 Discussion

In order to further improve the drilling efficiency of laser-assisted mechanical rock breaking, the beneficial effect of the laser should be fully used. However, the above studies have shown that different laser parameters produce different rock-breaking effects, which have implications for joint rock-breaking techniques. Therefore, the differences between the melting pit dominant mode and the thermal cracks dominant mode in joint rock-breaking effect are compared. Based on better drilling results, a more suitable dominant mode for assisted mechanical rock breaking is obtained, which in turn provides suggestions and guidance for the engineering application of laser-assisted mechanical rock breaking.

For assisted rock-breaking in the melting pit dominant mode, the laser first irradiates the forward rock and produces a conical melting pit hole, then the bit squeezes and scrapes the damaged rock to achieve intact rock breakage. In this process, the combined effect of drill thrust and cutting forces leads to stress concentrations around the melting pit hole, which reduces the difficulty of breaking the rock and reduces the force on the bit. But compared to conventional bit sizes (generally 80–120 mm in diameter), the melting pit hole is small and the impact area is difficult to cover the full cross-section of the bit, so this mode has limited improvement in combined drilling efficiency (Xu et al. 2022). For assisted rock breaking in the thermal cracks dominant mode, the laser first irradiates produces melting pit holes, and the holes are accompanied by crack network extending into space. The cutting teeth of the bit rotate and scrape the damaged rock,

**Fig. 15** Rock damage morphology at the end of uniaxial compression test. **a** 2400 W, 10 s, **b** 4800 W, 10 s



eventually producing a blocky rock chips flake, which facilitates a reduction in load on the cutting teeth and a significant increase in specific energy. Thus, the thermal cracks dominant mode is more conducive to the improvement of laser-assisted rock-breaking efficiency.

This feature should be fully considered when designing new combined laser-mechanical drilling bits, and the laser parameters in the thermal cracks dominant mode should be selected as far as possible to achieve a better combined drilling effect. When laser-mechanical combined drilling technology is used to break granite, it is recommended to use a laser power greater than 2400 W. However, the excessive laser power requires a larger laser cutting head, which poses a challenge to the internal space arrangement of the combined drill. In addition, although the high-power laser can cause a further decrease in the strength of the rock, the rate of decrease is not significant. Future combined laser-mechanical drilling bits design should fully consider the rock-breaking benefits and core component design space issues, and use these to select the optimal laser parameter range.

## 6 Conclusion

Uniaxial compression tests are conducted on laser-irradiated granite specimens, and the strength and deformation characteristics of the irradiated specimens are analyzed. The failure mode and rock strength weakening mechanism of the irradiated specimens are discussed in combination with the melting pit hole morphology and crack expansion path, finally, the selection of rock-breaking parameters and engineering recommendations for laser-assisted drilling are given. Based on this study, some main conclusions can be drawn as follows:

1. As the laser power increases, the peak stress of the specimen first decreases rapidly and then slowly in a linear trend, the peak strain increases approximately with an exponential trend, and the elastic modulus decreases approximately with a logarithmic trend. At the same time, the compaction and yield phase of the stress–strain curve are extended, and the behavior eventually transform from brittle damage to plastic damage.
2. The melting pit hole and crack network produced by irradiation are the root cause of the weakness of the compressive strength of the rock. Under axial load conditions, on one hand, melting pit holes can be seen as a conical free surface and the tip of the hole is prone to stress concentration; on the other hand, thermal cracks produce symmetric tensile cracks and forms damage surfaces, leading to weakening of the rock strength.

3. When the laser power does not exceed 2400 W, the effect of the melting pit hole on specimen cracking is greater than the effect of thermal cracks, and the specimen occurs splitting-tensile damage. When the laser power is greater than 2400 W, the effect of thermal cracks on specimen cracking is gradually greater than the effect of melting pit holes, and the specimen is more likely to occur block spalling damage. The thermal cracks dominant mode is more conducive to improving the rock-breaking efficiency of laser-assisted mechanical rock breaking, so when designing the new laser-assisted mechanical bit, in order to achieve better drilling effects on high-strength granite ground, a laser power exceeding 2400 W is required.

**Acknowledgements** This paper is funded by the National Natural Science Foundation of China (No. 42272311, 52021005), the Key Research and Development Plan of Shandong Province (No. 2020ZLYS01, 2022CXPT016), National Natural Science Youth Fund (No. 52309134), Shandong Province Natural Science Youth Fund (No. ZR2023QE266) and Laser Assisted Intelligent and Efficient Drilling and Tunneling Technology and Equipment (No. 1410121062).

**Funding** This paper is funded by the National Natural Science Foundation of China (No. 42272311, 52021005, 52309134), the Key Research and Development Plan of Shandong Province (No. 2020ZLYS01, 2022CXPT016), Natural Science Youth Foundation of Shandong Province (No. ZR2023QE266). No external funding was used.

**Data Availability** The data that support the findings of this study are available from the corresponding author upon reasonable request.

## Declarations

**Conflict of Interest** The authors declare that they have no conflicts of interest relevant to this work.

## References

- Ai T, Zhang R, Zhou HW, Pei JL (2014) Box-counting methods to directly estimate the fractal dimension of a rock surface. *Appl Surf Sci* 314:610–621
- Allaart P, Jones T (2023) Box-counting dimension and differentiability of box-like statistically self-affine functions. *J Math Anal Appl* 521(2):126909
- Atlasov R, Nikolaeva M, Karamzin V (2019) Development of drilling and casing technologies for permafrost areas. *IOP Conf Ser: Earth Environ Sci* 272(2):022078
- Cai M, Hou PY, Zhang XW, Fang XT (2021) Post-peak stress–strain curves of brittle hard rocks under axial-strain-controlled loading. *Int J Rock Mech Min Sci* 147:104921
- Capik M, Yilmaz AO (2021) Development models for the drill bit lifetime prediction and bit wear types. *Int J Rock Mech Min Sci* 139:104633
- Chen K, Huang ZQ, Deng R, Zhang WL, Kang MQ, Ma YC (2022a) Numerical simulation and test investigation on phase transition and thermal cracking process of sandstone by laser drilling. *Rock Mech Rock Eng* 55(4):2129–2147

- Chen K, Huang ZQ, Deng R, Zhang WL, Kang MQ, Ma YC, Shi MJ, Yan J (2022b) Research on the temperature and stress fields of elliptical laser irradiated sandstone, and drilling with the elliptical laser-assisted mechanical bit. *J Pet Sci Eng* 211:110147
- Dai XW, Huang ZW, Zou WC, Wu XG, Shi HZ (2021) Failure characteristics of rocks subjected to PDC cutter indentation. *J Pet Sci Eng* 207:108992
- Fan XD (2019) Study on the technical problems and countermeasures of PDC bits in the drilling process of Triassic mudstone. *West Resour* 3:5 (In Chinese)
- Fang TC, Ren FS, Wang BJ, Cheng JX, Liu HX (2021) Particle jet impact deep-rock in rotary drilling: failure process and lab experiment. *PLoS ONE* 16(4):e0250588
- Guo CG, Sun Y, Yue HT, Li Q, He SZ, Zhang JZ, Zhang Y (2022) Experimental research on laser thermal rock breaking and optimization of the process parameters. *Int J Rock Mech Min Sci* 160:105251
- Gupta A, Chattopadhyaya S, Hloch S (2013) Critical investigation of wear behaviour of WC drill bit buttons. *Rock Mech Rock Eng* 46:169–177
- Han YN, Li XR, Feng YC (2020) A new approach to evaluate rock drillability of polycrystalline diamond compact bits using scratch test data. *Energy Explor Exploit* 38(4):884–904
- Khaled MS, Chen MH, Losoya EZ, Rodriguez LA, Gildin E, Skelton RE (2022) Tensegrity laboratory drilling rig for earth and space drilling, mining, and exploration. *Int J Solids Struct* 252:111785
- Kirli MS, Fahrioglu M (2019) Sustainable development of Turkey: deployment of geothermal resources for carbon capture, utilization, and storage. *Energy Sources Part A-Recovery Util Environ Eff* 41(14):1739–1751
- Li B, Hu MM, Zhang B, Li NB, Shao W, Nie LC, Cao WZ, Xu B (2022a) Numerical simulation and experimental studies of rock-breaking methods for pre-grooving-assisted disc cutter. *Bull Eng Geol Environ* 81(3):90
- Li B, Zhang B, Hu MM, Liu B, Cao WZ, Xu B (2022) Full-scale linear cutting tests to study the influence of pre-groove depth on rock-cutting performance by TBM disc cutter. *Tunn Undergr Space Technol* 122:104366
- Li J, Du Q, Sun CX (2009) An improved box-counting method for image fractal dimension estimation. *Pattern Recognit* 42(11):2460–2469
- Li J, Peng SJ, Xu J, Yan FZ, Zhou J, Chen JR (2022c) Novel multi-field coupling high-voltage electric pulse fracturing coal-rock permeability enhancement test system. *Int J Rock Mech Min Sci* 158:105180
- Li MY, Han B, Zhang Q, Zhang SY, He QK (2019) Investigation on rock breaking for sandstone with high power density laser beam. *Optik* 180:635–647
- Li Y, Chen ZJ, Ye YH, Yang YX (2021a) Combined finite-discrete element method for modeling the interaction between single PDC cutter and brittle rock. *J Pet Sci Eng* 207:109133
- Li YL, Peng JM, Zhang PY, Huang CY (2021b) Hard rock fragmentation in percussion drilling considering confining pressure: insights from an experimental study. *Int J Rock Mech Min Sci* 148:104961
- Liu B, Zhang J, Wang JH, Li WX, Li SA (2020) Technologies for the safe and efficient drilling of ultradeep wells in the areas with intrusive rocks in the Shunbei Oilfield. *Oil Drill Prod Technol* 42(2):5 (In Chinese)
- Liu B, Hu MM, Zhang B, Li B, Xu B, Huang C, Yu H, Zhang JC, Gu LQ (2023) Influence of abrasive waterjet pre-cutting slit on the performance of shield cutter cutting reinforced concrete. *Tunn Undergr Space Technol* 142: 105448
- Lu GM, Feng XT, Li YH, Zhang XW (2019) The microwave-induced fracturing of hard rock. *Rock Mech Rock Eng* 52:3017–3032
- Lu YY, Tang JR, Ge ZL, Xia BW, Liu Y (2013) Hard rock drilling technique with abrasive water jet assistance. *Int J Rock Mech Min Sci* 60:47–56
- Maeda M, Kushiyama K (2005) Use of compact shield tunneling method in urban underground construction. *Tunn Undergr Space Technol* 20(2):159–166
- Martin CD, Chandler NA (1994) The progressive fracture of Lac du Bonnet granite. *Int J Rock Mech Min Sci Geotech Abstr* 31(6):643–659
- Ndeda R, Sebusang SEM, Marumo R, Ogur EO (2017) On the role of laser pulses on spallation of granite. *Lasers Manuf Mater Process* 4:60–75
- Pooniwala S (2006) Lasers: the next bit. In: SPE Eastern regional meeting. OnePetro
- Ren FS, Fang TC, Cheng XZ (2019) Theoretical modeling and experimental study of rock-breaking depth in particle jet impact drilling process. *J Pet Sci Eng* 183(1–2):106419
- Rui F, Zhao GF (2021) Experimental and numerical investigation of laser-induced rock damage and the implications for laser-assisted rock cutting. *Int J Rock Mech Min Sci* 139(7):104653
- Wang S, Xu Y, Xia KW, Tong TY (2020a) Dynamic fragmentation of microwave irradiated rock. *J Rock Mech Geotech Eng* 13(2):300–310
- Wang YJ, Jiang JY, Darkwa J, Xu ZY, Zheng XF, Zhou GQ (2020b) Experimental study of thermal fracturing of Hot Dry Rock irradiated by moving laser beam: temperature, efficiency and porosity. *Renew Energy* 160:803–816
- Xu BL, Liu SY, Li HS (2022) Drill string's axial force transfer law in slide directional drilling in underground coal mine. *Tunn Undergr Space Technol* 130:104701
- Xu Y, Yao W, Wang S, Xia KW (2020) Investigation of the heat-treatment effect on rock fragmentation characteristics using the dynamic ball compression test. *Rock Mech Rock Eng* 53(5):2095–2108
- Yang JP, Chen WZ, Yang DS, Yang DS, Tian HM (2016) Estimation of elastic moduli of non-persistent fractured rock masses. *Rock Mech Rock Eng* 49:1977–1983
- Yang SQ, Ranjith PG, Jing HW, Tian WL, Ju Y (2017) An experimental investigation on thermal damage and failure mechanical behavior of granite after exposure to different high temperature treatments. *Geothermics* 65:180–197
- Yin TB, Li XB, Cao WZ, Xia KW (2015) Effects of thermal treatment on tensile strength of Laurentian granite using Brazilian test. *Rock Mech Rock Eng* 48:2213–2223
- Zhang Y, Tao LJ, Liu J, Xu Z, Fei G, Lei T, Wang ZQ (2023) Construction techniques and mechanical behavior of newly-built large-span tunnel ultra-short distance up-crossing the existing shield tunnel with oblique angle. *Tunn Undergr Space Technol* 138:105162
- Zhao ZH (2016) Thermal influence on mechanical properties of granite: a microcracking perspective. *Rock Mech Rock Eng* 49:747–762
- Zhou XP, Chen JW (2019) Extended finite element simulation of step-path brittle failure in rock slopes with non-persistent en-echelon joints. *Eng Geol* 250:65–88
- Zhou XP, Zhang T, Qian QH (2021) A two-dimensional ordinary state-based peridynamic model for plastic deformation based on Drucker-Prager criteria with non-associated flow rule. *Int J Rock Mech Min Sci* 146:104857
- Zhou YQ, Sheng Q, Li NN, Fu XD (2020) The influence of strain rate on the energy characteristics and damage evolution of rock materials under dynamic uniaxial compression. *Rock Mech Rock Eng* 53:3823–3834
- Zhu XH, Luo YX, Liu WJ, Hu H, Chen MQ (2022) Numerical electric breakdown model of heterogeneous granite for electro-pulse-boring. *Int J Rock Mech Min Sci* 154:105128

**Publisher's Note** Springer Nature remains neutral with regard to jurisdictional claims in published maps and institutional affiliations.

Springer Nature or its licensor (e.g. a society or other partner) holds exclusive rights to this article under a publishing agreement with the author(s) or other rightsholder(s); author self-archiving of the accepted manuscript version of this article is solely governed by the terms of such publishing agreement and applicable law.